EUROPEAN ORGANIZATION FOR NUCLEAR RESEARCH

CERN-SL-2000-012 AP
CERN-NUFACT-NOTE 22

# Fringe Fields, Dynamic Aperture and Transverse Depolarisation in the CERN Muon Storage Ring

**F. Zimmermann**

**Abstract**

We evaluate the dynamic aperture for the CERN muon storage ring, and, in particular, study the effect of magnet fringe fields. The detuning with amplitude is computed via normal-form analysis. Particle tracking reveals the dependence of the dynamic aperture on betatron tune and momentum offset, and demonstrates satisfactory performance. The depolarisation in transverse phase space is estimated from a spin normal form. All calculations are performed with the computer codes COSY INFINITY and MAD.

Geneva, Switzerland

May 4, 2000

# 1 Introduction

In this paper, we investigate the effect of fringe fields and the dynamic aperture in the muon storage ring [1] of the CERN neutrino factory. Earlier similar studies for the FNAL design revealed a strong reduction of the dynamic aperture due to quadrupole fringe fields [2, 3, 4]. The transverse normalised beam emittance in the CERN muon storage ring is assumed to be 1.7 mm mrad, half as large as for the FNAL design. At 50 GeV, this corresponds to a geometric emittance of about 7 $\mu$m, or to beam sizes of a few centimeters. The rms energy spread is 0.5%, again half the FNAL value. An acceptance of $3\sigma$ over a few hundred turns is desirable in both transverse phase space and momentum.

The CERN ring is of triangular shape and includes three straight sections, two of which are used as neutrino production straights aimed at distant detectors. The magnets in the straight sections are weakly focusing and the beta functions are large in order to confine the beam divergence. The arcs exhibits stronger focusing and much smaller beta functions. The magnet apertures vary roughly with the beam size. Quadrupole bore radii are 89 mm in the straight sections, and 31 mm in the arcs. Pole tip fields are 0.5 T and 3 T, respectively, and quadrupole lengths 0.35 m in the straight and 0.5 m in the arcs. The arc dipole field is 6 T. The arcs are equipped with sextupoles for chromatic correction. Table 1 summarises the relevant parameters. The exponential decay time of the muons corresponds to about 150 turns.

Table 1: Some parameters of the CERN muon storage ring [5].

| | | |
|---|---|---|
| beam energy | $E$ | 50 GeV |
| normalised emittance | $\gamma\epsilon_{x,y}$ | 1.7 mm rad |
| rms energy spread | $(\Delta p/p)_{\rm rms}$ | 0.5% |
| circumference | $C$ | 2068.8 m |
| betatron tunes | $Q_{x,y}$ | 11.250, 12.203 |
| arc quad radius | $r_a$ | 31 mm |
| arc quad pole tip | $B_{T,a}$ | 3 T |
| arc quad length | $l_a$ | 0.5 m |
| arc dipole field | $B$ | 6 T |
| arc dipole length | $l$ | 2.9 m |
| straight-section quad radius | $r_p$ | 89 mm |
| straight-section quad pole tip | $B_{T,p}$ | 0.5 T |
| straight-section quad length | $l_p$ | 0.35 m |

In COSY the fringe field fall off near the magnet edge can be described by a so-called Enge function [6, 7],

$$F(z) = \frac{1}{1 + \exp(a_1 + a_2(z/D) + \ldots + a_6(z/D)^6)}, \tag{1}$$

which characterises the variation of the dipole or quadruple field with longitudinal position $z$ along the magnet axis. The scaling parameter $D$ is the diameter of the magnet bore. The default Enge coefficients represent measurements of a family of PEP magnets [8]. For example, in case of a

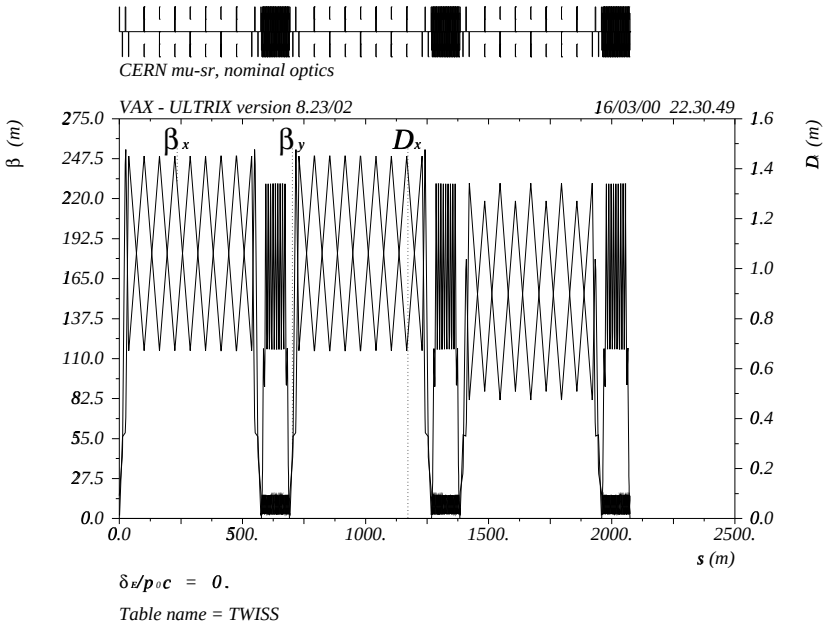


Figure 1: Optics of the CERN muon storage ring [5].

quadrupole, these coefficients are $a_1 = 0.296417$, $a_2 = 4.533219$, $a_3 = -2.270982$, $a_4 = 1.068627$, $a_5 = -0.036391$, and $a_6 = 0.022261$. A different set of coefficients was inferred from TOSCA simulations for a spectrometer magnet at GSI [9], namely $a_1 = 0.1122$, $a_2 = 6.2671$, $a_3 = -1.4982$, $a_4 = 3.5882$, $a_5 = -2.1209$, and $a_6 = 1.723$. Figure 2 compares the quadrupole-field fall off for these two parametrisations.

## 2 Results

A COSY input file of the muon storage ring was created from the MAD lattice [5] using the MAD-to-COSY converter [10]. The fractional betatron tunes computed by COSY are $Q_x = 0.2500$, and $Q_y = 0.2028$ [1], and agree with the tunes from MAD [12]. The simulations include three different types of nonlinearities: fringes, sextupoles and kinematic corrections.

Figure 3 shows the horizontal and vertical phase space obtained by tracking for 1000 turns (trajectories are plotted on every 5th turn) through a 9th order Taylor map representing the entire muon-storage ring with nonlinear kinematic terms, fringe fields and chromatic-correction sextupoles. The vertical axis is the horizontal or vertical slope of the particle trajectory, $x'$ or $y'$, in units of rad, and the horizontal axis is the transverse position, $x$ or $y$, in units of meter. The observation point is at the center of a defocusing quadrupole in one of the straight sections. All trajectories in Fig. 3 are regular,

[1] Recently, the nominal tunes of the muon storage ring were set to the LHC injection tunes, $Q_x = 0.28$ and $Q_y = 0.31$ [11].

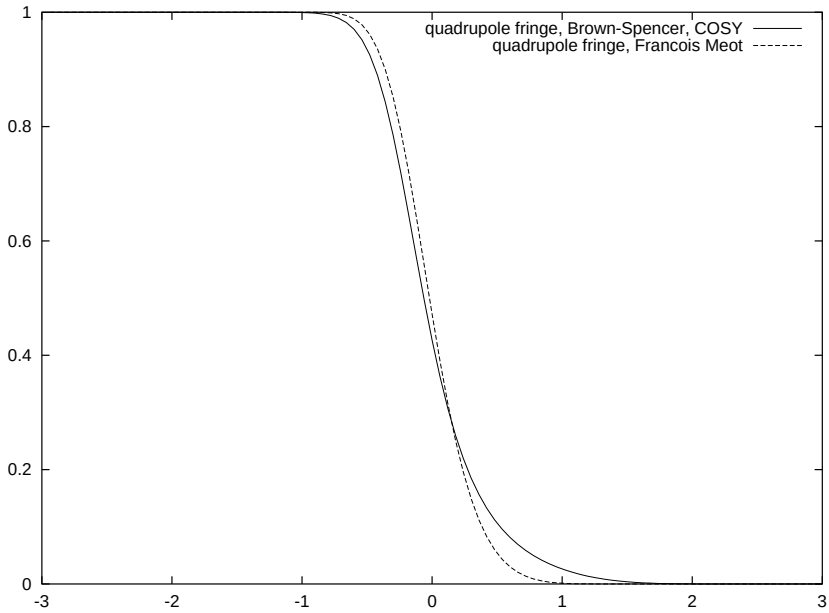


Figure 2: The fall-off of a quadrupole fringe field as a function of the longitudinal distance from the magnet edge in units of the full magnet aperture, comparing two different models: COSY default (solid line) and alternative parametrisation of in Ref. [9]. In both cases, the fall-off is described by an Enge function $F(z)$, Eq. (1), with coefficients quoted in the text. An additional 10% change in the parameter $D$ for the second case was also taken into account.

and the dynamic aperture is well above the required $3\sigma$.

As discussed in Ref. [3], the tune shifts with amplitude can be obtained from a normal form analysis in COSY INFINITY. Table 2 lists the linear tune shifts with amplitude calculated by COSY for four cases: the full lattice including sextupoles and fringe fields, the lattice without fringe fields, the bare lattice, and finally, the full lattice with a different length for one of the critical matching quadrupoles (see subsequent discussion). The table shows that the kinematic terms are negligible, whereas the tune shifts induced by the fringe fields are of the same order of magnitude as those arising from the chromatic-correction sextupoles. This is also reflected by the size of the tune footprints, shown in Fig. 4.

The on-energy dynamic aperture for various betatron tunes is illustrated in Figs. 5 and 6. The trajectories revolve on regular elliptical orbits. Only near the quarter integer resonance we see an island structure, excited by the fringe fields.

For the FNAL muon storage ring, we have shown that quadrupole fringe fields in the matching section between arcs and production straight can cause a strong reduction of the dynamic aperture [3]. Also in the CERN storage ring design, the largest fringe field effect is expected to arise from the matching section, where the product of quadrupole gradient and squared beam size is much larger than in the arcs or straights. Figure 7 compares the horizontal phase space at a tune near the 4th integer resonance for two different lengths (and associated strengths) of matching quadrupole Q3M. The larger amplitude of the island position, in the right picture, indicates a stronger horizontal detuning

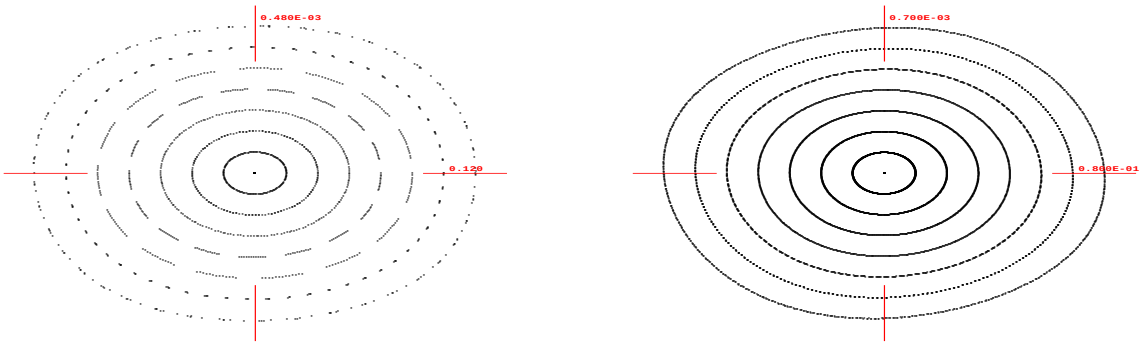


Figure 3: Horizontal (left) and vertical phase space (right), obtained by 9th order tracking through the muon storage ring, including nonlinear quadrupole fringe fields and chromatic-correction sextupoles. Beta functions at the observation point are $\beta_x = 249.65$ m, $\beta_y = 115.33$ m, fractional betatron tunes $Q_x = 0.294$ and $Q_y = 0.288$. Particles are launched in steps of about $0.5\sigma$, and the plot range extends over about $\pm 4\sigma$. The energy offset is zero.

with amplitude for the shorter quadrupole length. This is consistent with the linear detuning in Table 2. The optics of the matching section for the two quadrupole lengths are compared in Fig. 8. Except for the length of quadrupole Q3M, they are indistinguishable. The dependence of the fringe-field effect on quadrupole gradient and beta function can be understood from analytical considerations; see, *e.g.*, Ref. [4], and references therein. Fortunately, in this optics the fringe field effect is rather benign. It becomes visible only in the immediate vicinity of the 3rd or 4th order resonance.

As indicated in the introduction, the fall off of the magnetic field is not exactly known, until the magnets have been designed or built. To illustrate the sensitivity to the exact shape of the field fall off, Fig. 9 compares phase space plots computed with the standard COSY fringe field à la Brown and Spencer and for the alternative parametrisation proposed by Méot. The unperturbed tunes without

Table 2: Linear tune shift in various configurations, for fractional betatron tunes of $Q_x = 0.294$ and $Q_y = 0.288$. The bare lattice contains kinematic terms only.
$^\circ$ Length of matching quadrupole Q3M(T) reduced by a factor of two.

| tune shift | $dQ_x/dI_x$ | $dQ_x/dI_y$ | $dQ_y/dI_y$ |
|---|---|---|---|
| sexts. & fringe fields | 152 | $-68$ | 200 |
| sexts. w/o fringe fields | 44 | $-180$ | 104 |
| bare lattice | 5 | 3 | 5 |
| sexts. & fringe fields$^\circ$ | 186 | $-54$ | 200 |

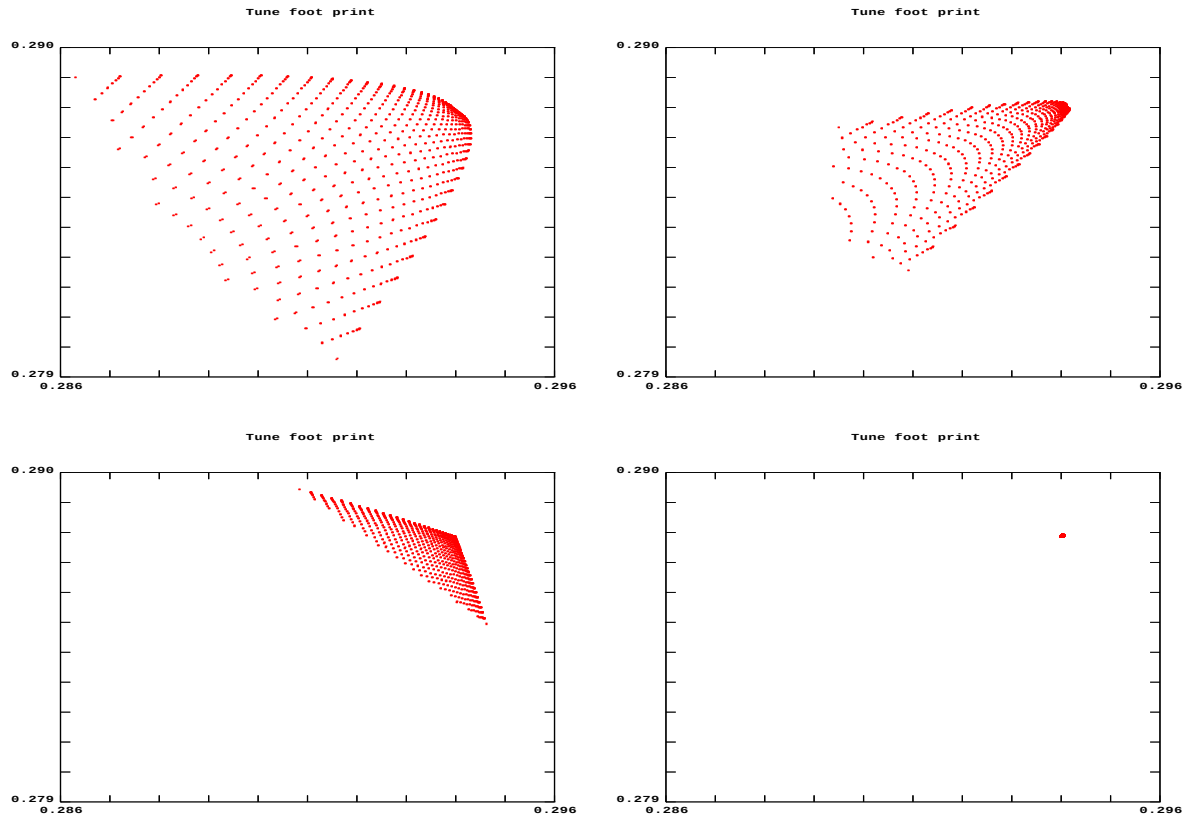


Figure 4: Tune foot print for horizontal and vertical starting amplitudes up to $3\sigma$, calculated from 5th order normal form. The two axes display the horizontal and vertical fractional tunes. Top left: full lattice including sextupoles and fringes; top right: only fringes; bottom left: full lattice including sextupoles but without fringe fields; bottom right: bare lattice.

fringe fields are 0.254455 and 0.28730. With the default COSY fringe field [8], on the left, the tunes are shifted to $Q_x = 0.24342$ and $Q_y = 0.27588$, whereas the tunes obtained using Méot's fringe field, in the right picture, are $Q_x = 0.22944$ and $Q_y = 0.26350$.

We recall that the energy acceptance of the ring should be as large as $\pm$1.5%. The next series of phase space plots illustrates the dynamic aperture for off-energy particles, obtained by tracking through an energy dependent 8th order map. Figures 10 and 11 depict the horizontal phase space for energy offsets of $-1.5$% and $+1.5$%, respectively, with various values of the horizontal tune spanning a total $Q_x$ range of 0.1. For tunes between the fourth and third integer resonance, the dynamic aperture is about 2–2.5$\sigma$. Figures 12 and 13 depict the equivalent pictures for the vertical plane. The next four figures, 14–17, are phase space plots for exactly the same conditions as the four previous figures, but calculated without any fringe fields. Except near low-order resonances, no limit on the dynamic aperture can now be seen within $4\sigma$. Thus, the fringe fields do have some influence on the dynamic aperture for off-energy particles.

However, when physical aperture restrictions are taken into account, the fringe-field effects may

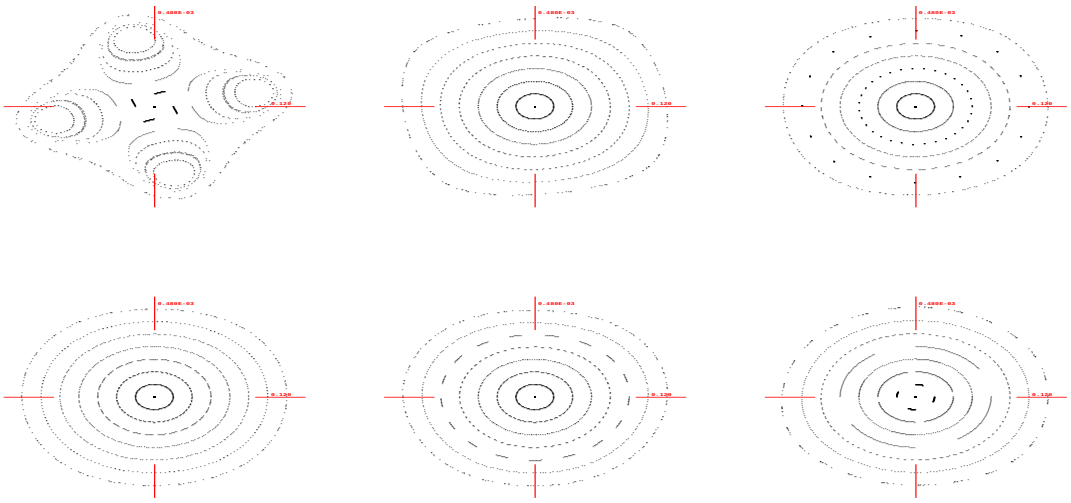

Figure 5: Horizontal phase space with 9th order map including sextupoles and fringe fields for several values of the horizontal tune, varying from 0.25 to 0.35 in steps of 0.02. Each plot extends over $\pm 4\ \sigma$.

no longer be relevant. This is demonstrated in Figs. 18 to 21, which again show the situation without fringe fields, this time simulated by MAD and including, at every magnet, a physical aperture of $3\sigma$, *i.e.*, three times the rms beam beam size. Evidently, the dynamic aperture induced by the fringe fields, as computed by COSY in Figs. 11 etc., lies outside the physical aperture.

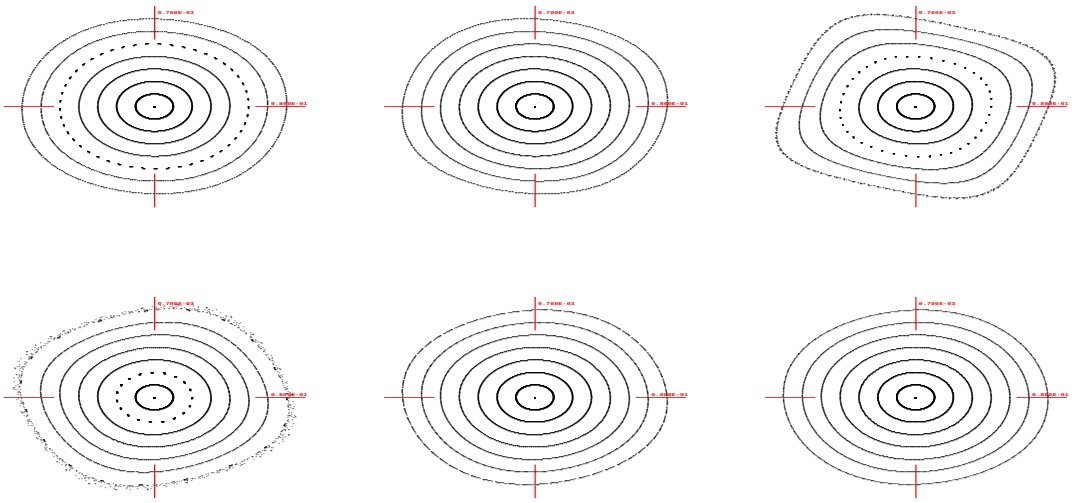

Figure 6: Vertical phase space with 9th order map including sextupoles and fringe fields for several values of the vertical tune, varying from 0.20 to 0.30 in steps of 0.02. Each plot extends over $\pm 4\ \sigma$.

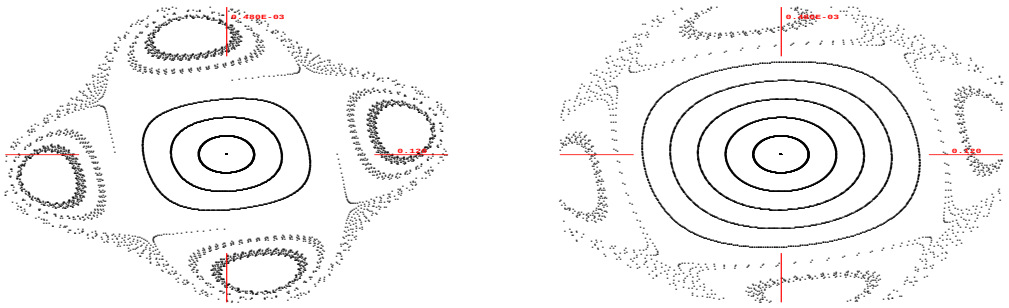

Figure 7: Horizontal phase space near the 4th integer resonance for two different lengths of Q3M, a quadrupole in the matching section, as obtained by 9th order tracking including chromatic-correction sextupoles and quadrupole fringe fields. Left: nominal optics with length of quadrupole Q3M equal to 2 m; right: Q3M length reduced to 1 m and corresponding increase in quadrupole gradient. The horizontal beta function at the observation point is $\beta_x = 250$ m. The horizontal tune is the same for the two cases: $Q_x = 0.254$. Particles are launched in steps of about $0.5\sigma$, and the plot range extends over $\pm 4\sigma$. The energy offset is zero.

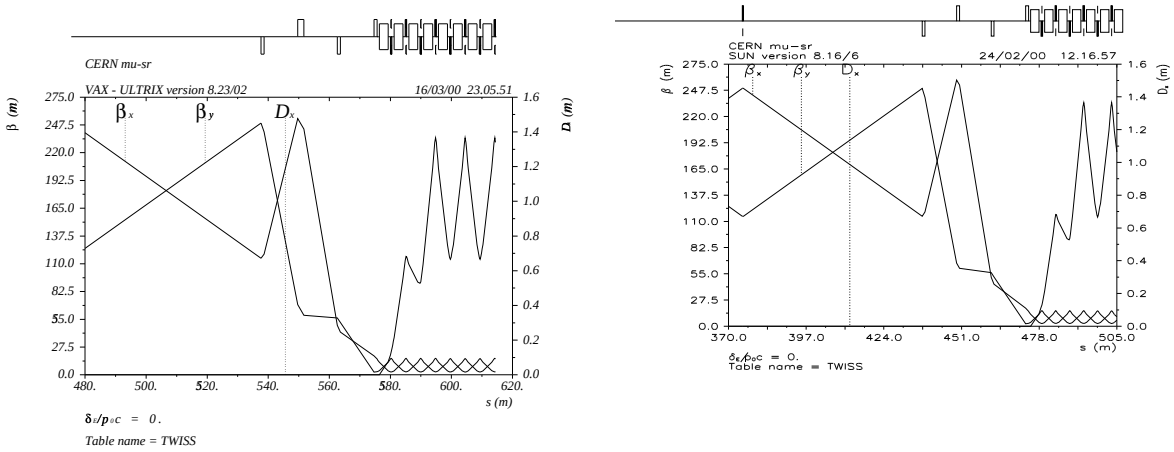


Figure 8: Optics of the matching section in the CERN muon storage ring; nominal (left) and an older version with shorter length of quadrupole Q3M (right) [5].

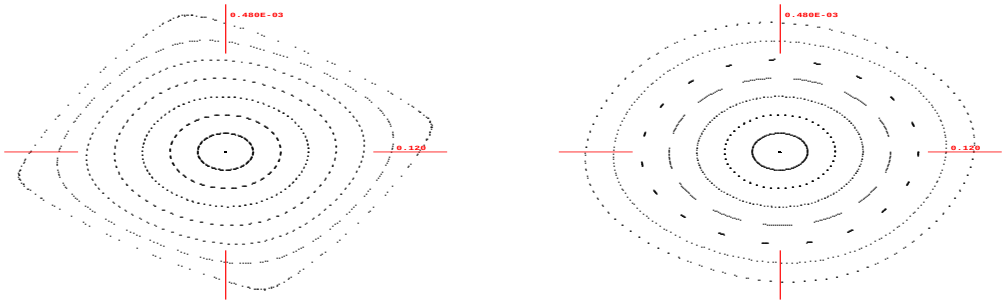


Figure 9: Horizontal phase space for two different parametrisations of the fringe-field fall-off, as given by Brown and Spencer (left) [8], and assumed by Méot (right) [9]. The tracking was performed with COSY INFINITY including the linear component of the fringe field (COSY option FR3), and considering the case with a shorter Q3M quadrupole length of 1 m. The horizontal beta function at the observation point is $\beta_x = 250$ m. The unperturbed tunes without fringe fields are 0.254455 and 0.28730, which are shifted to $Q_x = 0.24342$ and $Q_y = 0.27588$ (left), and $Q_x = 0.22944$ and $Q_y = 0.263495$ (right). In both cases, particles are launched in steps of about $0.5\sigma$, and the plot ranges extend over $\pm 4\sigma$. The energy offset is zero.

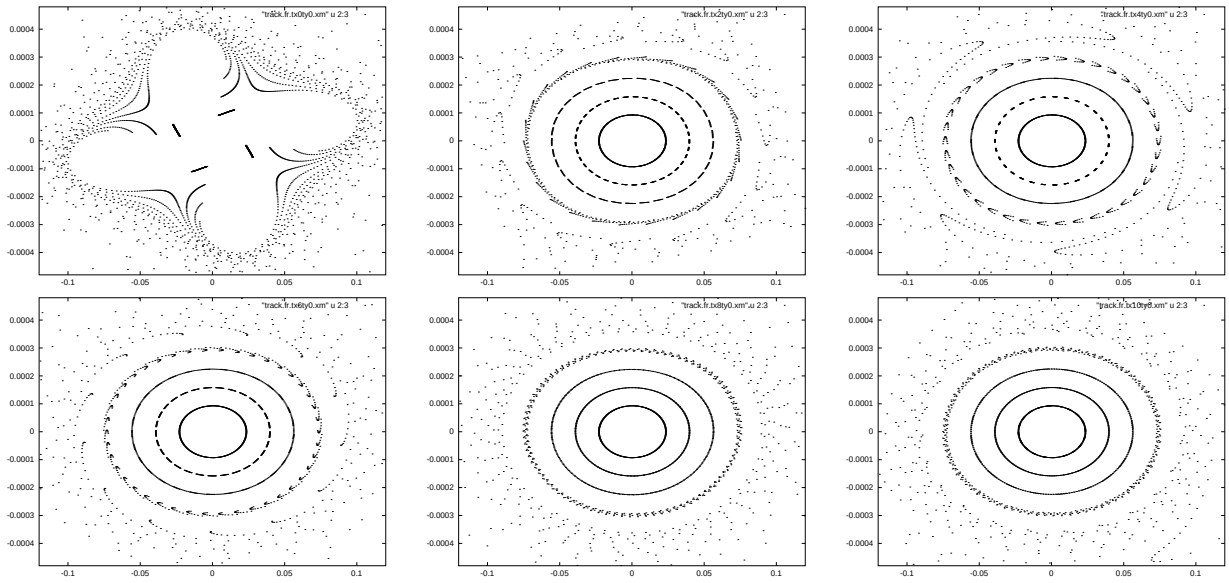

Figure 10: Horizontal phase space with 8th order map at a constant energy offset of $-1.5\%$ for several values of the horizontal tune, varying from 0.25 to 0.35 in steps of 0.02. Each plot extends over $\pm 4\ \sigma$. Fringe fields are included.

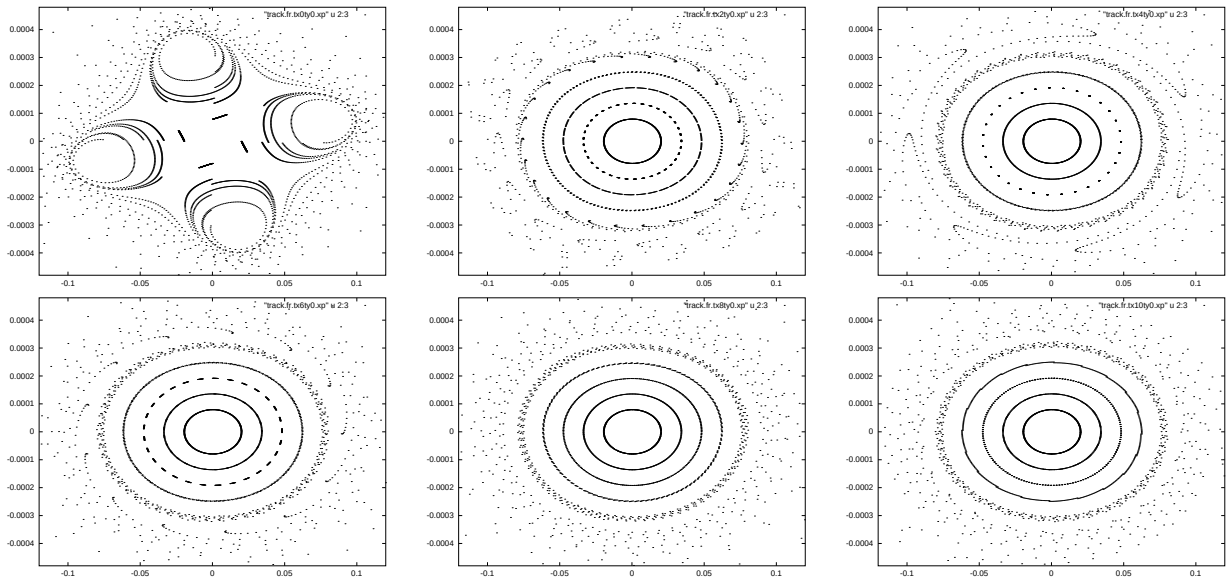

Figure 11: Horizontal phase space with 8th order map at a constant energy offset of $+1.5\%$ for several values of the horizontal tune, varying from 0.25 to 0.35 in steps of 0.02. Each plot extends over $\pm 4\ \sigma$. Fringe fields are included.

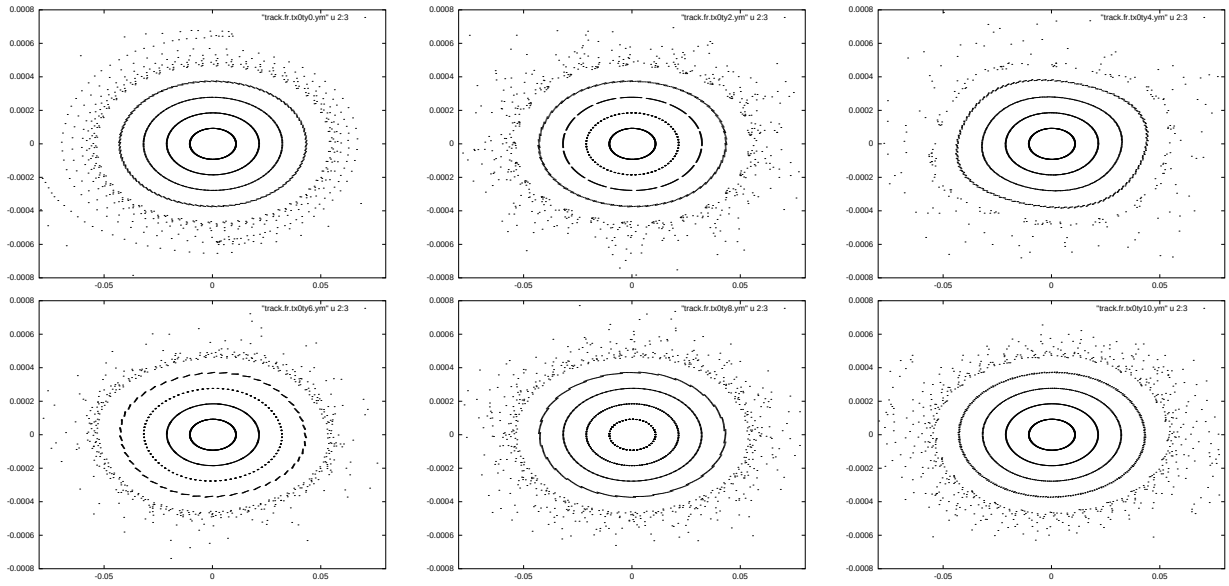


Figure 12: Vertical phase space with 8th order map at a constant energy offset of $-1.5\%$ for several values of the vertical tune, varying from 0.20 to 0.30 in steps of 0.02. Each plot extends over $\pm 4\ \sigma$. Fringe fields are included.

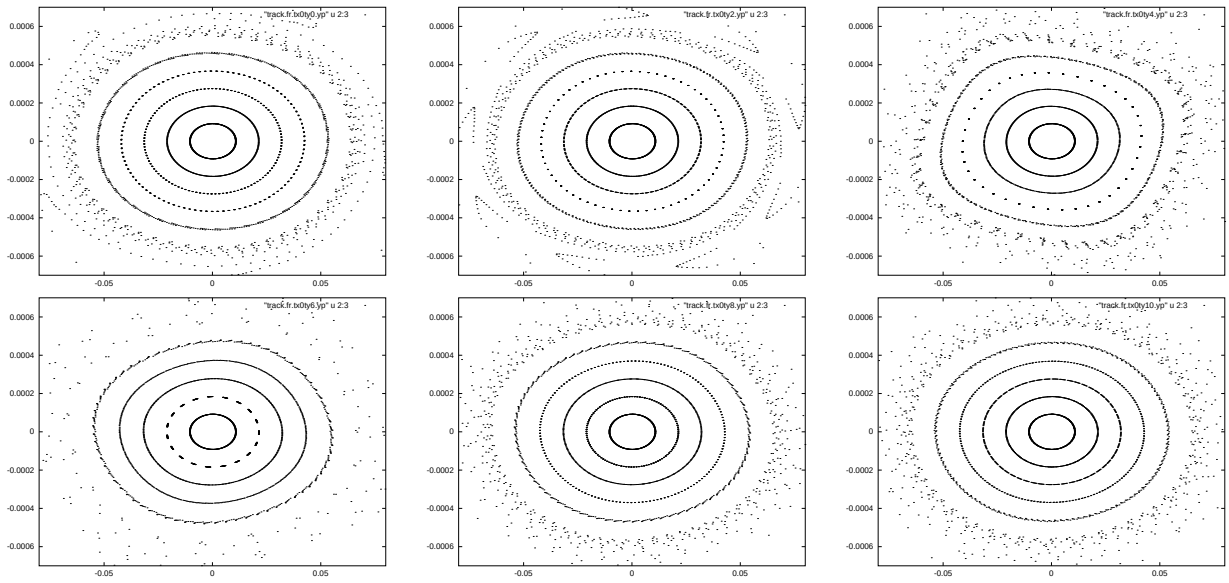


Figure 13: Vertical phase space with 8th order map at a constant energy offset of $+1.5\%$ for several values of the vertical tune, varying from 0.20 to 0.30 in steps of 0.02. Each plot extends over $\pm 4\ \sigma$. Fringe fields are included.

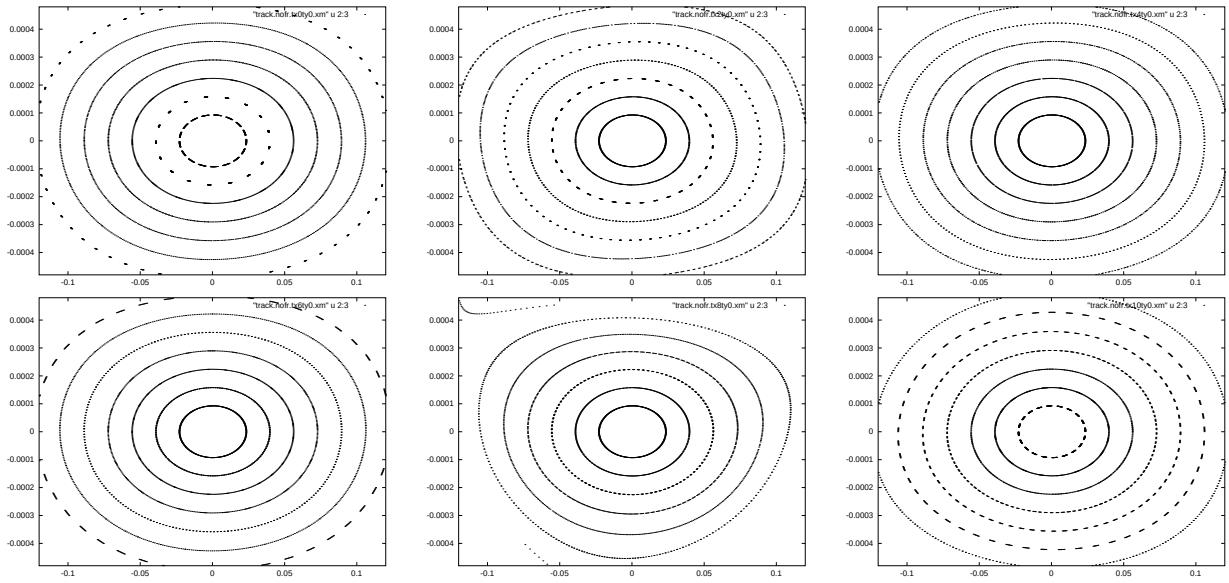

Figure 14: Horizontal phase space with 8th order map, not including fringe fields, at a constant energy offset of $-1.5\%$ for several values of the horizontal tune, varying from 0.25 to 0.35 in steps of 0.02. Each plot extends over $\pm 4\ \sigma$.

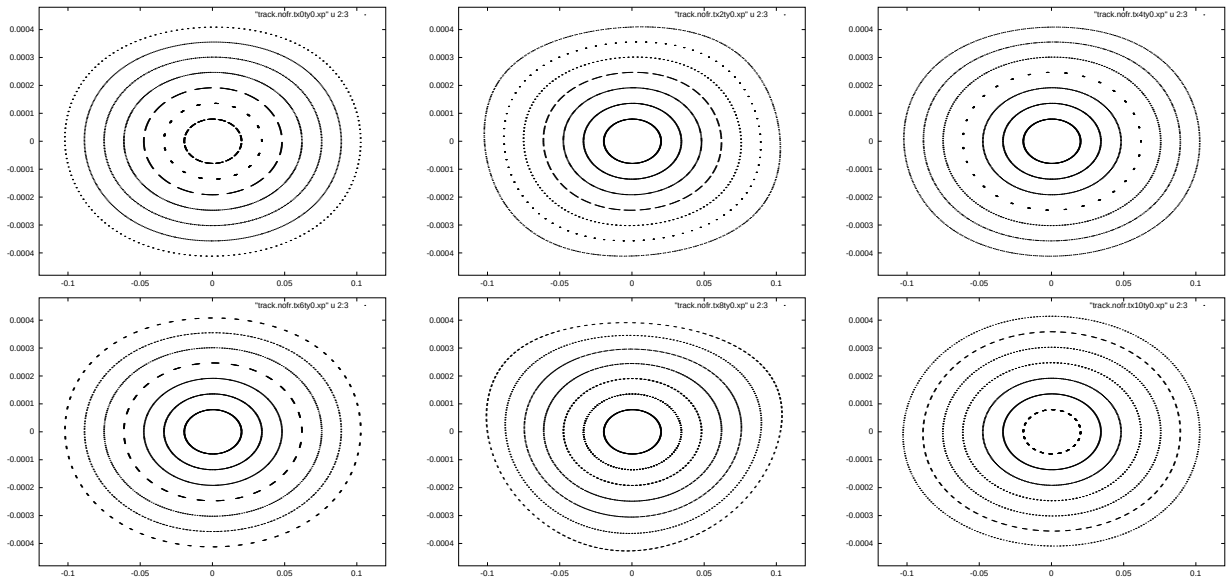

Figure 15: Horizontal phase space with 8th order map, not including fringe fields, at a constant energy offset of $+1.5\%$ for several values of the horizontal tune, varying from 0.25 to 0.35 in steps of 0.02. Each plot extends over $\pm 4\ \sigma$.

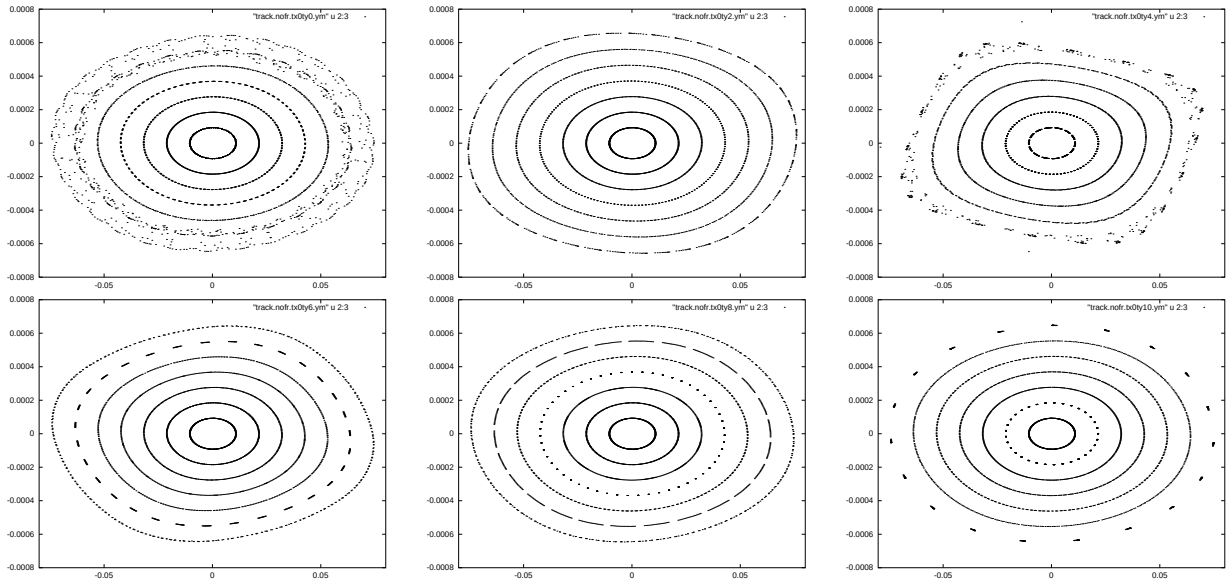


Figure 16: Vertical phase space with 8th order map, not including fringe fields, at a constant energy offset of $-1.5\%$ for several values of the vertical tune, varying from 0.20 to 0.30 in steps of 0.02. Each plot extends over $\pm 4\ \sigma$.

Finally, we look at the preservation of polarisation. The spin decoherence caused by different energies may be controlled via momentum compaction factor, rf frequency and rf voltage [13]. The spins can also decohere due to differences in the particle orbits. This second question is addressed in Fig. 22, which displays the variation of the $n$-axis and the variation in spin tune for trajectories extending up to $\pm 3\sigma$ in transverse phase space. The non-vertical components of the $n$ axis vary by less than 0.5%, and the spin tune only by about $1$–$2 \times 10^{-6}$. From this, we estimate that the net depolarisation due to the dependence of spin motion on transverse coordinates is considerably smaller than 1%.

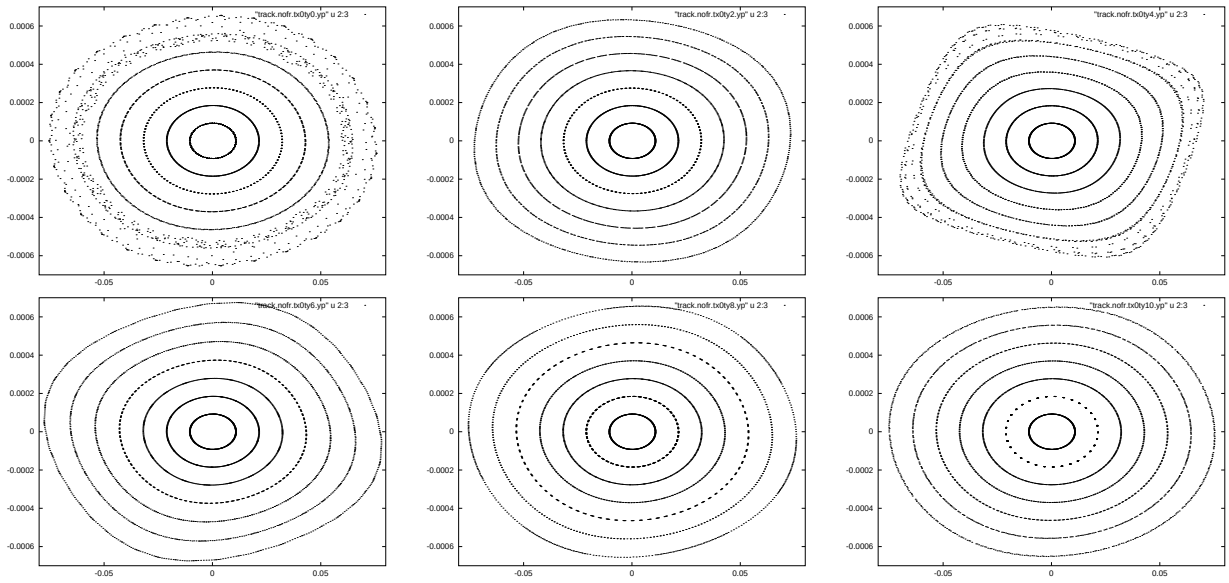


Figure 17: Vertical phase space with 8th order map, not including fringe fields, at a constant energy offset of $+1.5\%$ for several values of the vertical tune, varying from 0.20 to 0.30 in steps of 0.02. Each plot extends over $\pm 4\ \sigma$.

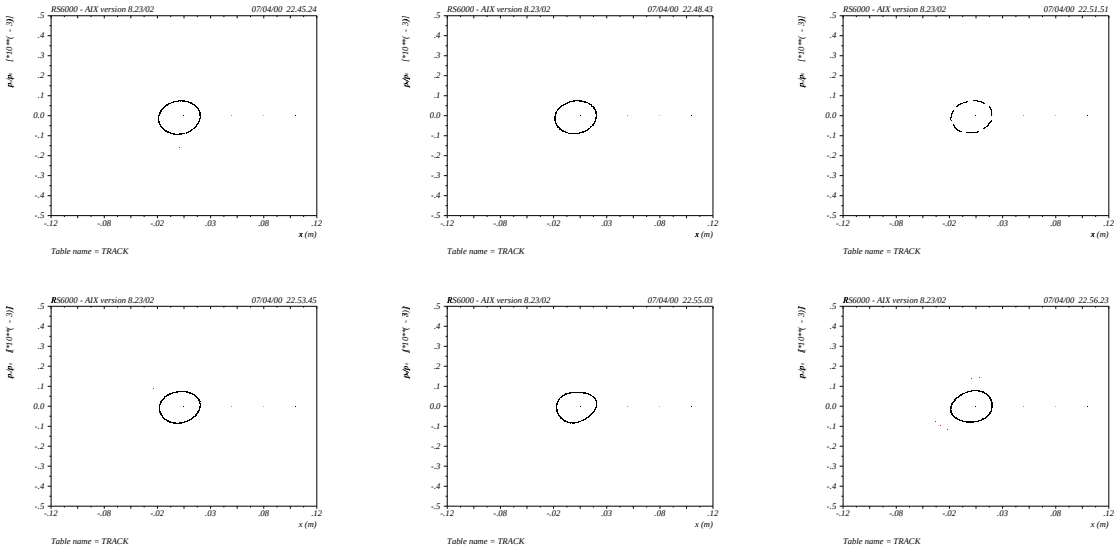


Figure 18: Horizontal phase space computed by MAD tracking at a constant energy offset of $-1.5\%$ for several values of the horizontal tune, varying from 0.25 to 0.35 in steps of 0.02, and with a physical aperture of $3\sigma$ at every magnet. Each plot extends over $\pm 4\ \sigma$. Fringe fields are not included.

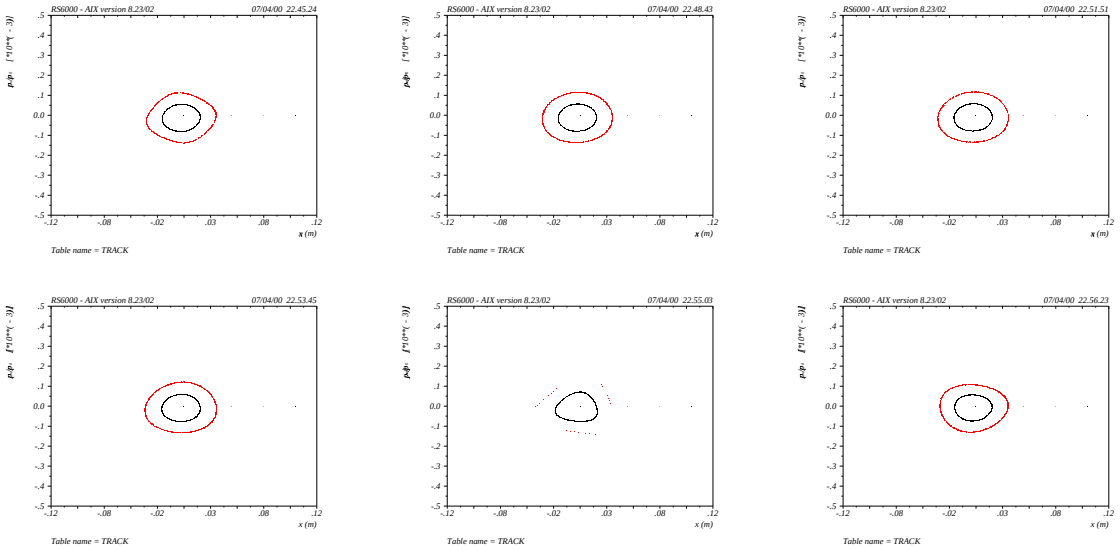


Figure 19: Horizontal phase space computed by MAD tracking at a constant energy offset of $+1.5\%$ for several values of the horizontal tune, varying from 0.25 to 0.35 in steps of 0.02, and with a physical aperture of $3\sigma$ at every magnet. Each plot extends over $\pm 4\ \sigma$. Fringe fields are not included.

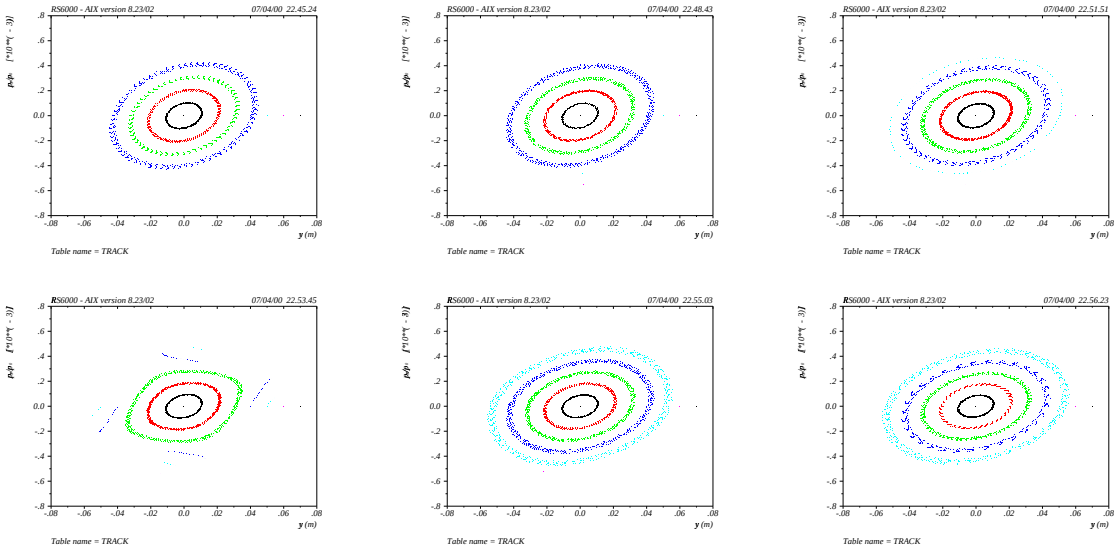


Figure 20: Vertical phase space computed by MAD tracking at a constant energy offset of $-1.5\%$ for several values of the vertical tune, varying from 0.20 to 0.30 in steps of 0.02, and with a physical aperture of $3\sigma$ at every magnet. Each plot extends over $\pm 4\ \sigma$. Fringe fields are not included.

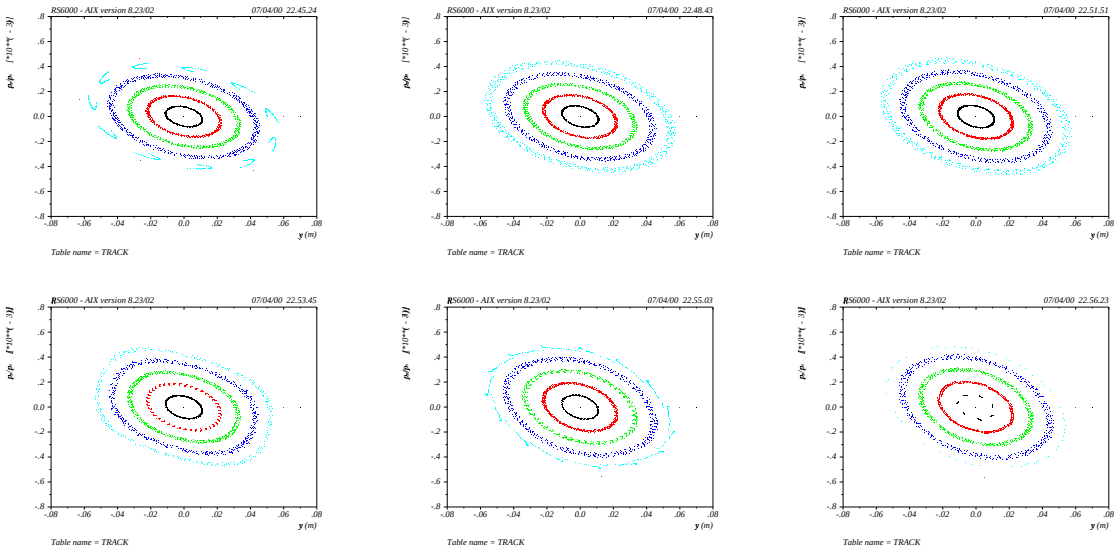


Figure 21: Vertical phase space by MAD tracking a constant energy offset of $+1.5\%$ for several values of the vertical tune, varying from 0.20 to 0.30 in steps of 0.02, with a physical aperture of $3\sigma$ at every magnet. Each plot extends over $\pm 4\ \sigma$. Fringe fields are not included.

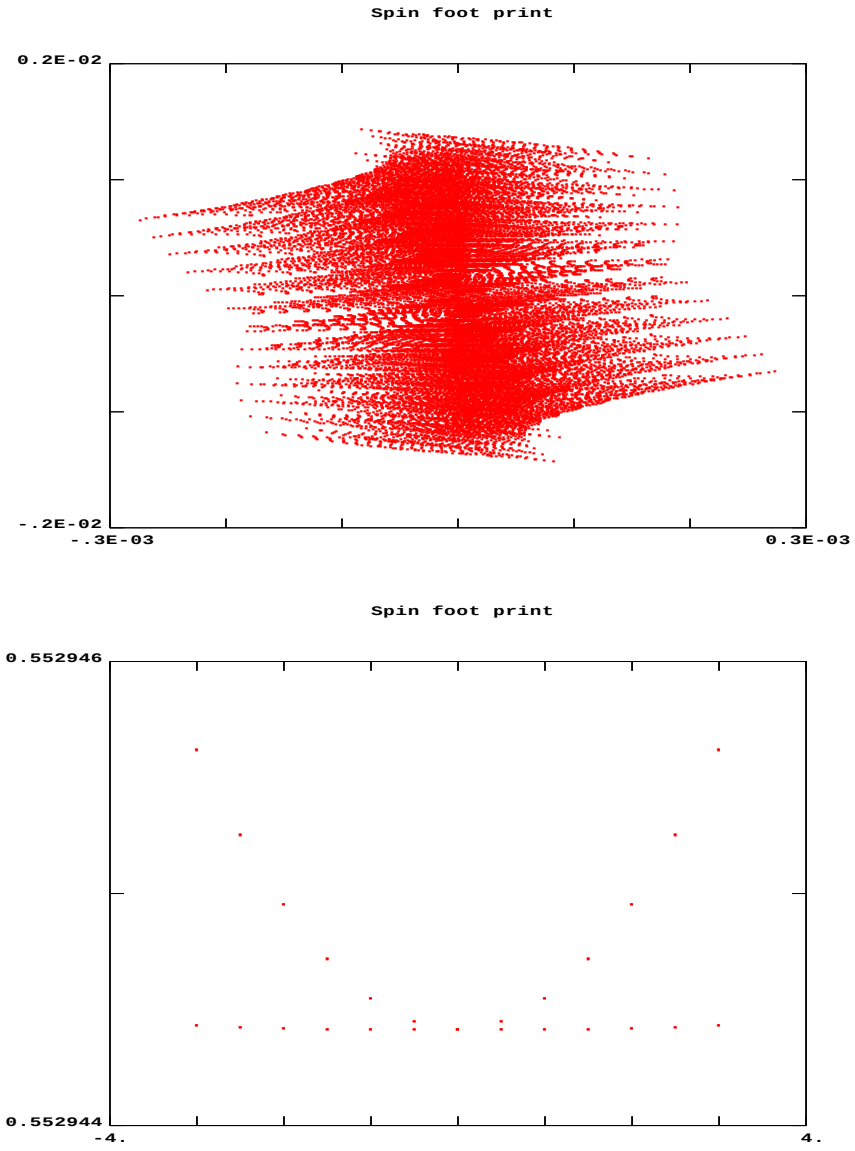


Figure 22: Spin footprints for the CERN muon storage ring. Shown are the longitudinal and horizontal components of the $n$-axis for transverse coordinates extending up to $\pm 3\sigma$ (top) and the spin tune [the rotation frequency around the $n$ axis] as a function of starting coordinates in units of $\sigma$ (bottom). The spin normal-form analysis was performed to 4th order.

## 3 Conclusions

The dynamic aperture of the CERN muon storage ring is larger than the physical aperture (chosen as 3 times the rms beam size) at almost all betatron tunes. This holds true even for the maximum momentum error of $\pm 1.5\%$. Fringe fields are marginally important in the matching section between arcs and straights, where they could affect the dynamic aperture if the quadrupole magnets are shortened or if the real field fall off of the magnets deviates largely from our assumption. The depolarisation due to the dependence of $n$ axis and spin tune on transverse coordinates is negligible.

## 4 Acknowledgements

I thank M. Berz, B. Erdelyi C. Johnstone, E. Keil, K. Makino, and F. Méot for discussions on fringe fields, and N. Holtkamp, E. Keil and F. Ruggiero for their support and encouragement.

## References

[1] E. Keil, talks held at FNAL (03.12.99) and at CERN (12.01.00), web site: 'http://wwwslap.cern.ch/~keil/talk.html'.

[2] M. Berz, K. Makino, B. Erdelyi, "Fringe Field Effects in Muon Rings", Proc. of HEMC'99 workshop on muon colliders at highest energies, Montauk, Long Island (1999).

[3] F. Zimmermann, C. Johnstone, M. Berz, B. Erdelyi, K. Makino, W. Wan, "Fringe Fields and Dynamic Aperture in the FNAL Muon Storage Ring", CERN Report CERN-SL-2000-011 AP and CERN-NUFACT-NOTE 21 (2000).

[4] F. Zimmermann, "Tune Shift with Amplitude Induced by Quadrupole Fringe Fields", CERN Report CERN-SL-2000-009 AP and CERN-NUFACT-NOTE 18 (2000).

[5] E. Keil, private communications, and talk at ~keil/MuMu/Doc/NFWG/03dec99.pdf

[6] M. Berz et al., COSY INFINITY web page. http://cosy.nscl.msu.edu

[7] "COSY INFINITY. Version 8. User's Guide and Reference Manual", MSUCL-1088 revised (1999).

[8] K. Brown and J. Spencer, "Non-linear Optics for the Final Focus of the Single-Pass Collider", IEEE Tr. N. Sc. NS-28, 3, p. 2568 (1981).

[9] F. Méot, "On the effect of fringe fields in the CERN 50 GeV muon storage ring", unpublished.

[10] The MAD-to-COSY converter was written by R. Servranckx.

[11] E. Keil, private communication.

[12] H. Grote and F. C. Iselin, "The MAD program (methodical accelerator design) version 8.4: User's reference manual," CERN-SL-90-13-AP-REV.2 (1990).

[13] R. Raja, "The effect of RF on polarization in a muon storage ring", FNAL Muon Collider Note 77 (2000).